Supporting Information

How Does the Fluorination of the Linker Affect the Stability of Trimesate-Based Coordination Polymers and MOFs?

John Krautwurst[†], Daniel Smets[†], Rainer Lamann[†], and Uwe Ruschewitz[*,†]

[†] Department of Chemistry, University of Cologne, Greinstraße 6, D-50939 Cologne, Germany

Description of determination of torsion angles and search within the CSD database to identify possible candidates for the synthesis of isostructural series with different degrees of fluorination

Determination of torsion angles. Within the Diamond software[1] a first plane was defined using all six carbon atoms of the phenyl ring and a second plane by the three atoms of the carboxylate group. Using the "Measure Planes" option the angle between these two planes was determined, which is given as the torsion angle in this work.

Search within the CSD database to identify possible candidates for the synthesis of isostructural series with different degrees of fluorination. To restrict the search within the CSD database[2] to reasonable candidate structures a recently defined subset with approx. 70.000 MOF structures[3] was used. Using the Conquest search module[4] of the CSD database ca. 1000 entries were identified, which contain the trimesate linker (1,3,5-benzenetricarboxylate). In a first step these entries were examined more or less randomly using the visualization option within Conquest to identify candidate structures with torsion angles between the phenyl ring and the carboxylate groups, which are significantly larger than 0°. Using this approach we identified $^{3}_{\infty}[Ba(HBTC)(H_2O)_2]\cdot ½\ H_2O$[5] and UHM-33[6] as interesting candidates, which are described in the main body of this manuscript. At the moment we are working on improvements of this approach by using a parser (M. Cullmann, Bachelor Thesis, Cologne, **2018**), written in Python 3[7], which allows a more systematic analysis of the subsets described above.

References:

[1] Brandenburg, K. *Diamond 3.2i*, Crystal Impact GbR, Bonn, Germany, **2012**.

[2] Groom, C. R.; Bruno, I. J.; Lightfoot M. P.; Ward, S. C. The Cambridge Structural Database. *Acta Crystallogr.* **2016**, *B72*, 171-179.

[3] Moghadam, P. Z.; Li, A.; Wiggin, S. B.; Tao, A.; Maloney, A. G. P.; Wood, P. A.; Ward, S. C.; Fairen-Jimenez, D. Development of a Cambridge Structural Database Subset: A Collection of Metal–Organic Frameworks for Past, Present, and Future. *Chem. Mater.* **2017**, *29*, 2618-2625.

[4] Bruno, I. J.; Cole, J. C.; Edgington, P. R.; Kessler, M.; Macrae, C. F.; McCabe, P.; Pearson, J.; Taylor, R. New software for searching the Cambridge Structural Database and visualising crystal structures. *Acta Crystallogr.* **2002**, *B58*, 389-397.

[5] Plater, M. J.; Roberts, A. J.; Marr, J.; Lachowski, E. E.; Howie, R. A. Hydrothermal synthesis and characterisation of alkaline-earth metal salts of benzene-1,3,5-tricarboxylic acid. *Dalton Trans.* **1998**, 797-802.

[6] Peikert, K.; Hoffmann, F.; Fröba, M. Fluorine magic: one new organofluorine linker leads to three new metal–organic frameworks. *CrystEngComm* **2015**, *17*, 353-360.

[7] van Rossum, G. Python reference manual, Centrum voor Wiskunde en Informatica (CWI). 1995. – CWI Report R9525.

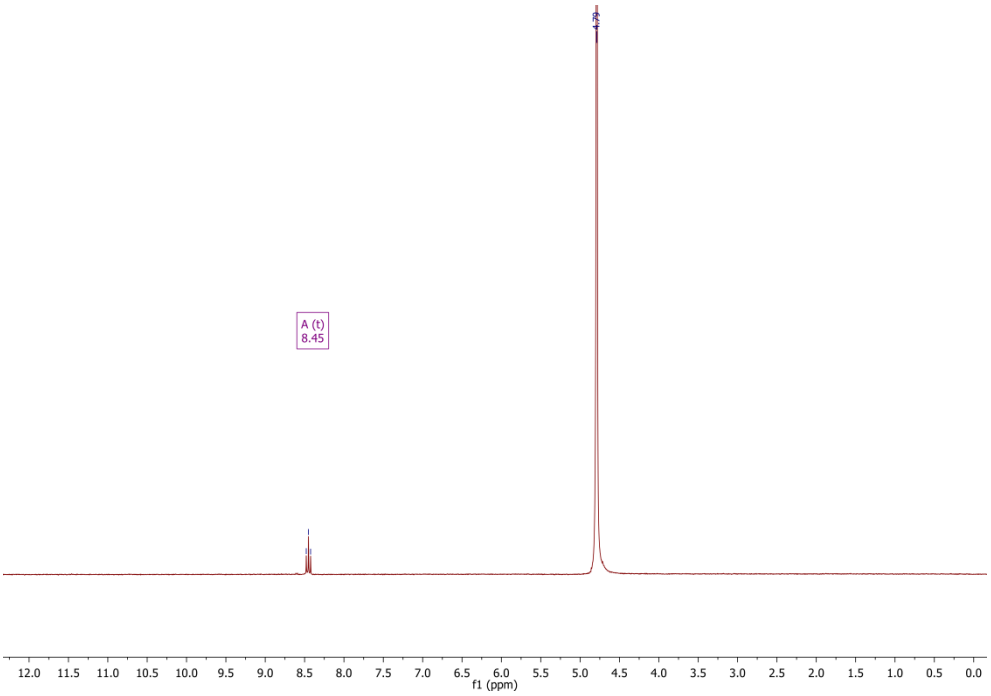

Figure S1. ^{1}H NMR spectrum of K(H_2*dF*-BTC) (**1**) in D_2O (H_2O: 4.79 ppm).

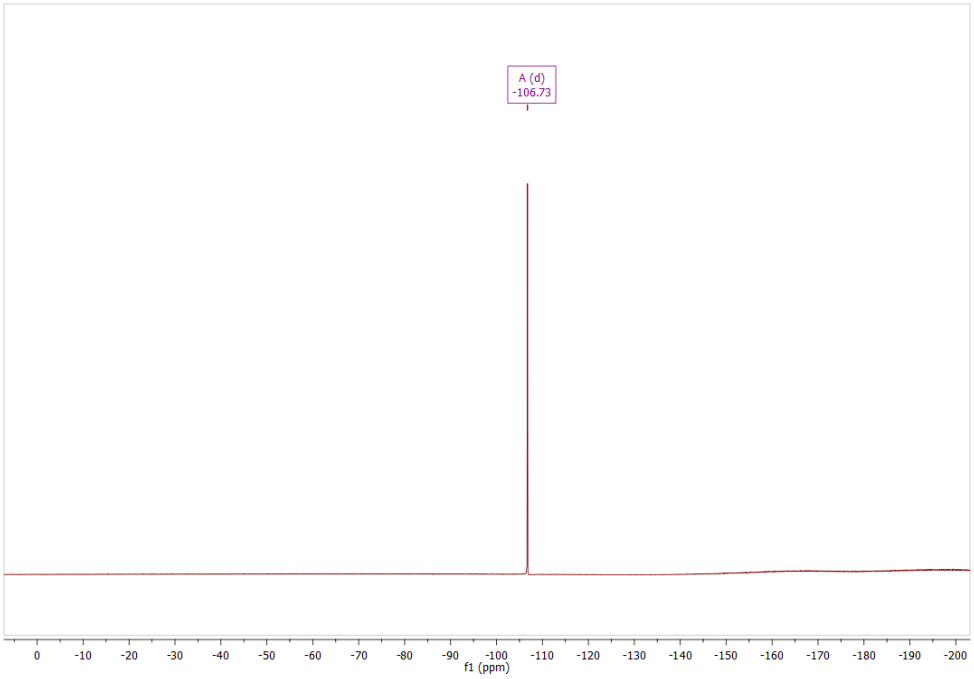

Figure S2. ^{19}F NMR spectrum of K(H_2*dF*-BTC) (**1**) in D_2O.

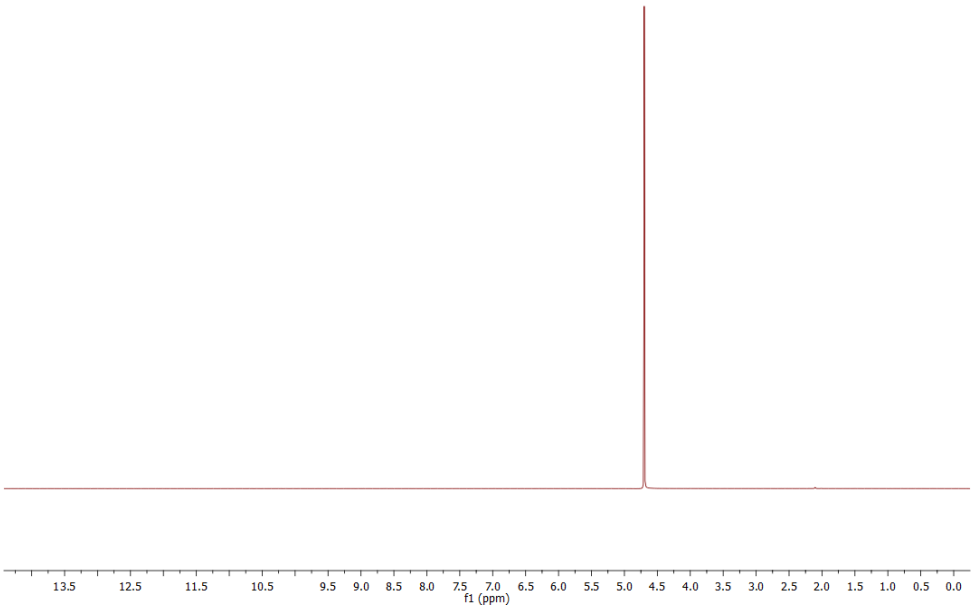

Figure S3. ^{1}H NMR spectrum of K(H_2*pF*-BTC) (**2**) in D_2O (H_2O: 4.79 ppm).

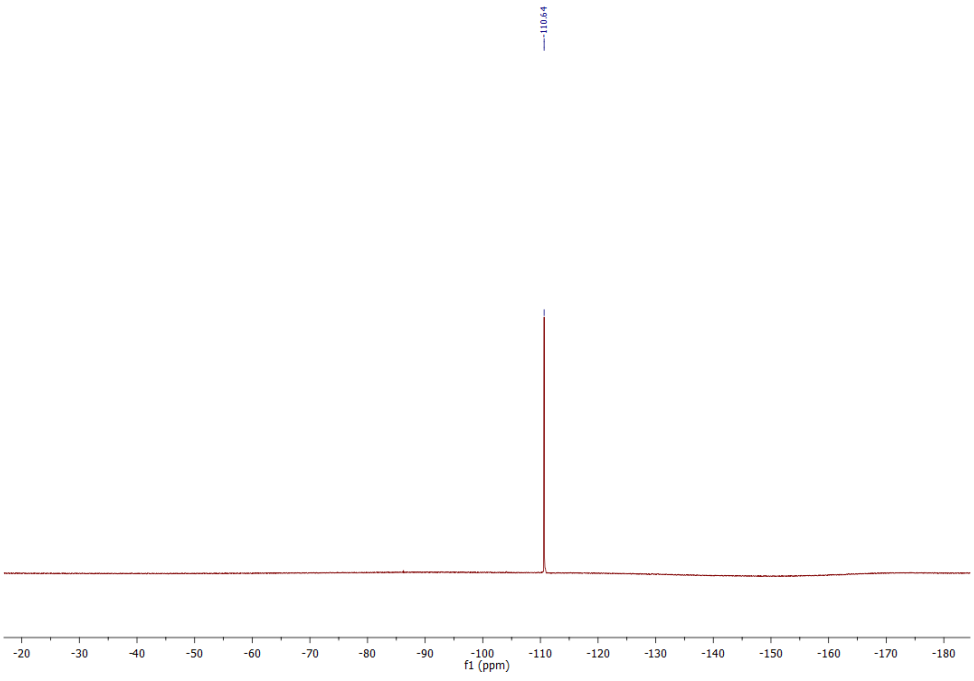

Figure S4. ^{19}F NMR spectrum of K(H_2*pF*-BTC) (**2**) in D_2O**.**

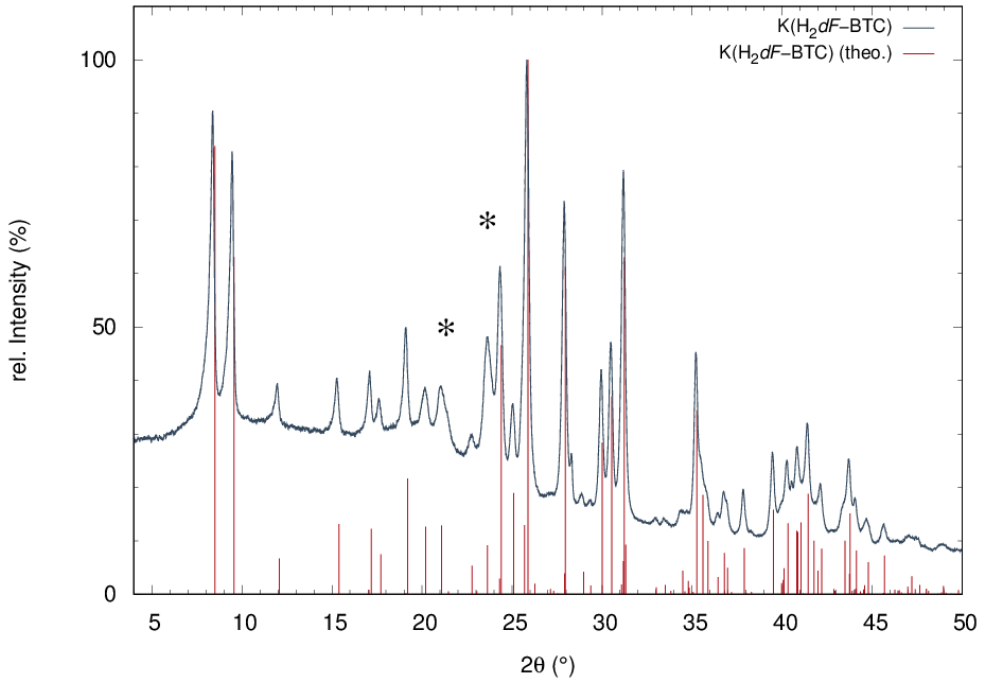

Figure S5. XRPD pattern of K(H_2*dF*-BTC) (**1**) (blue curve; Huber G670, Cu-$K_{\alpha 1}$ radiation). For comparison the theoretical pattern calculated from single crystal data is shown (red line diagram). Reflections of the sample holder are marked with a "*".

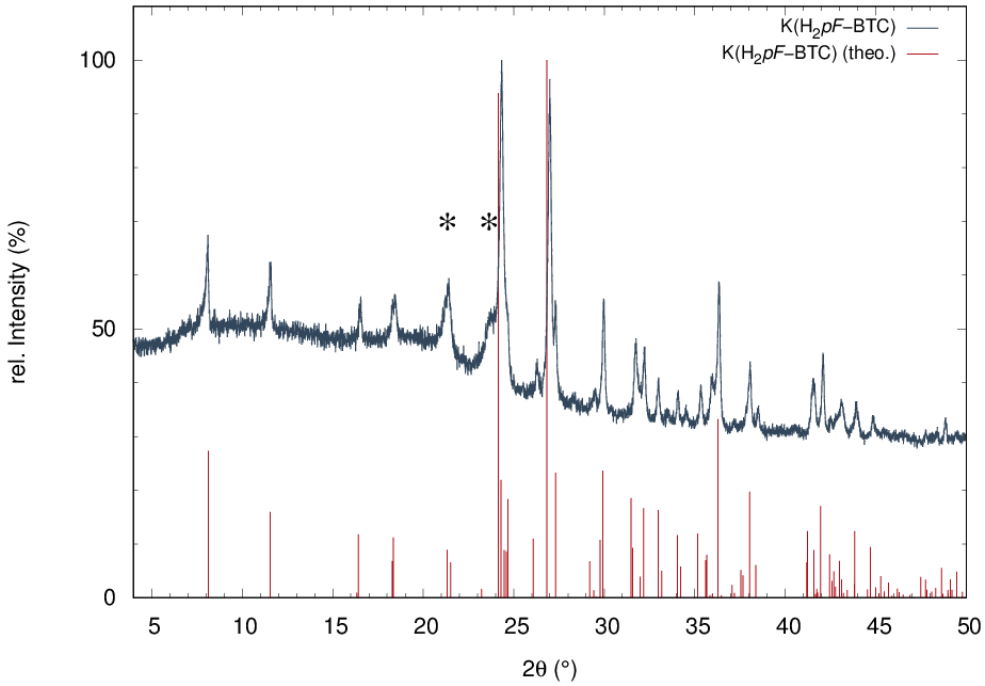

Figure S6. XRPD pattern of K(H_2*pF*-BTC) (**2**) (blue curve; Huber G670, Cu-$K_{\alpha 1}$ radiation). For comparison the theoretical pattern calculated from single crystal data is shown (red line diagram). Reflections of the sample holder are marked with a "*".

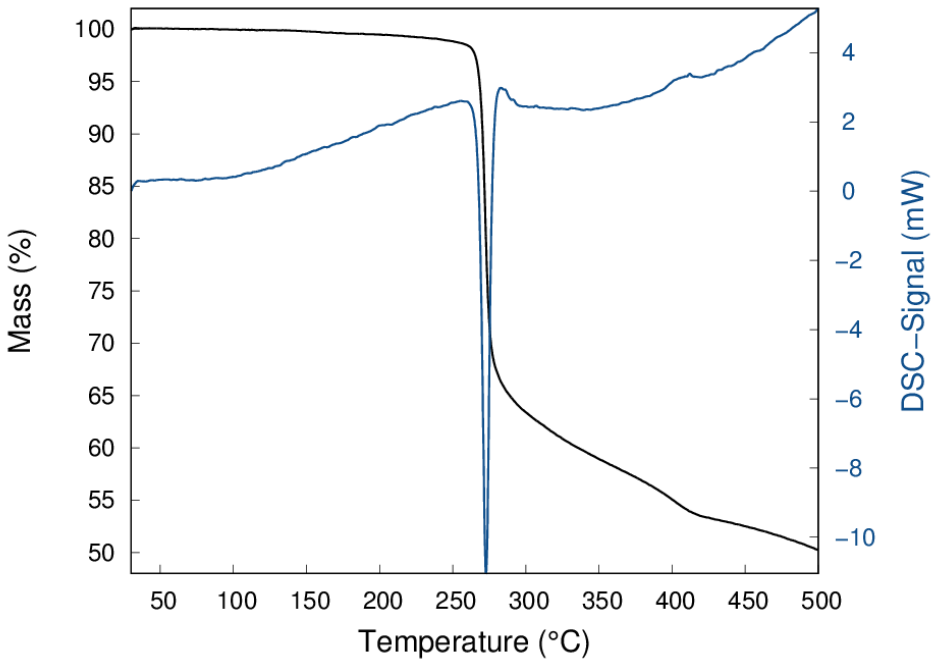

Figure S7. DSC (blue) and TGA (black) curves of K(H_2*dF*-BTC) (**1**).

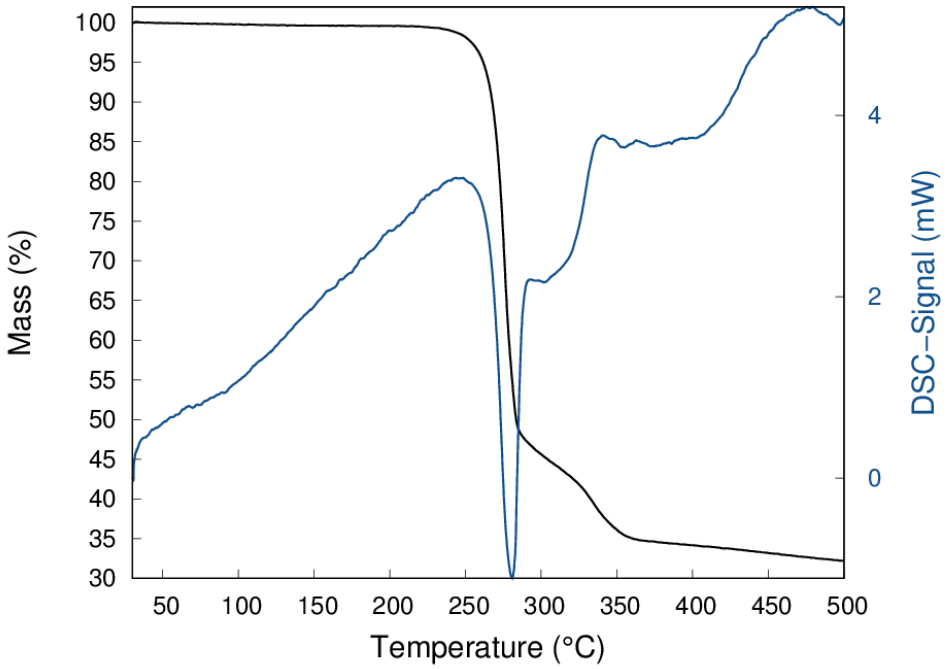

Figure S8. DSC (blue) and TGA (black) curves of K(H_2*pF*-BTC) (**2**)

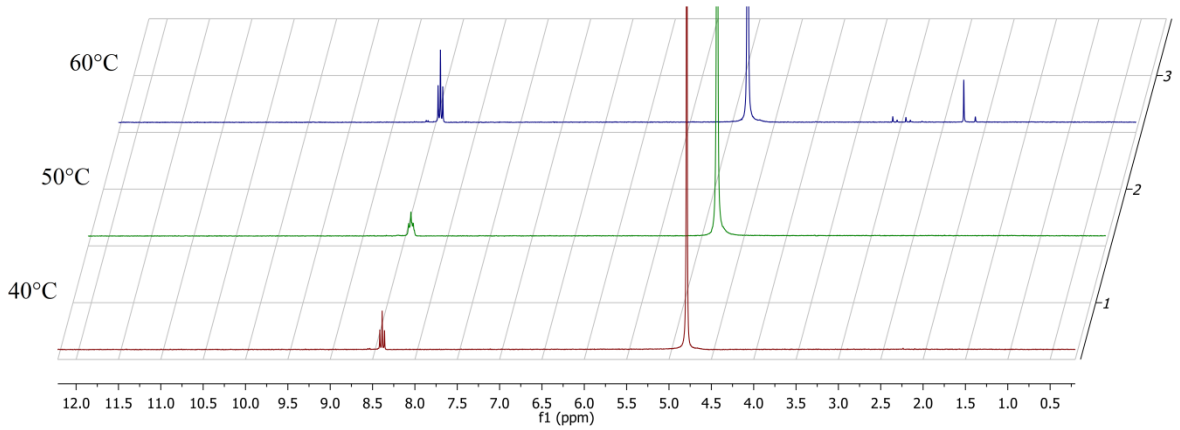

Figure S9. ^{1}H NMR spectra of K(H_2*dF*-BTC) (**1**) after heating in D_2O at different temperatures (H_2O: 4.79 ppm).

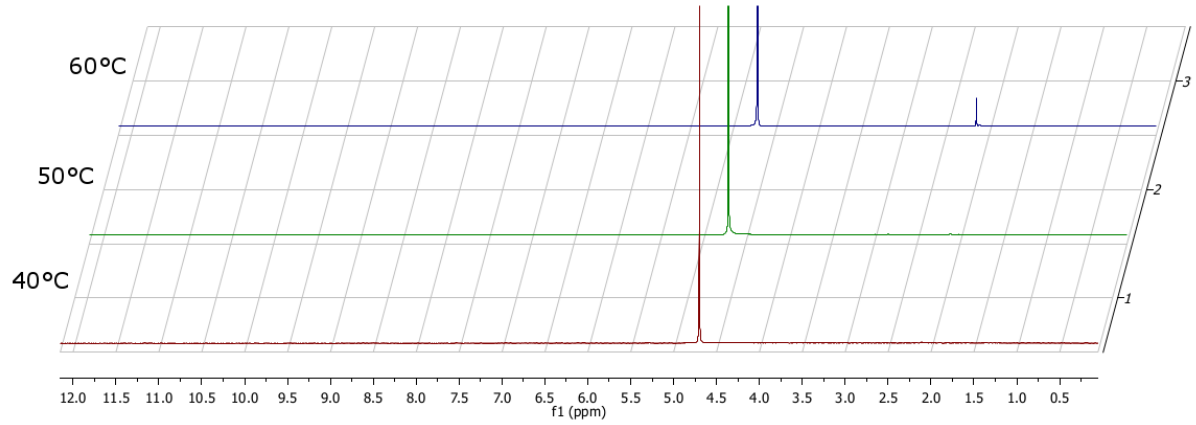

Figure S10. ^{1}H NMR spectra of K(H_2*pF*-BTC) (**2**) after heating in D_2O at different temperatures (H_2O: 4.79 ppm).

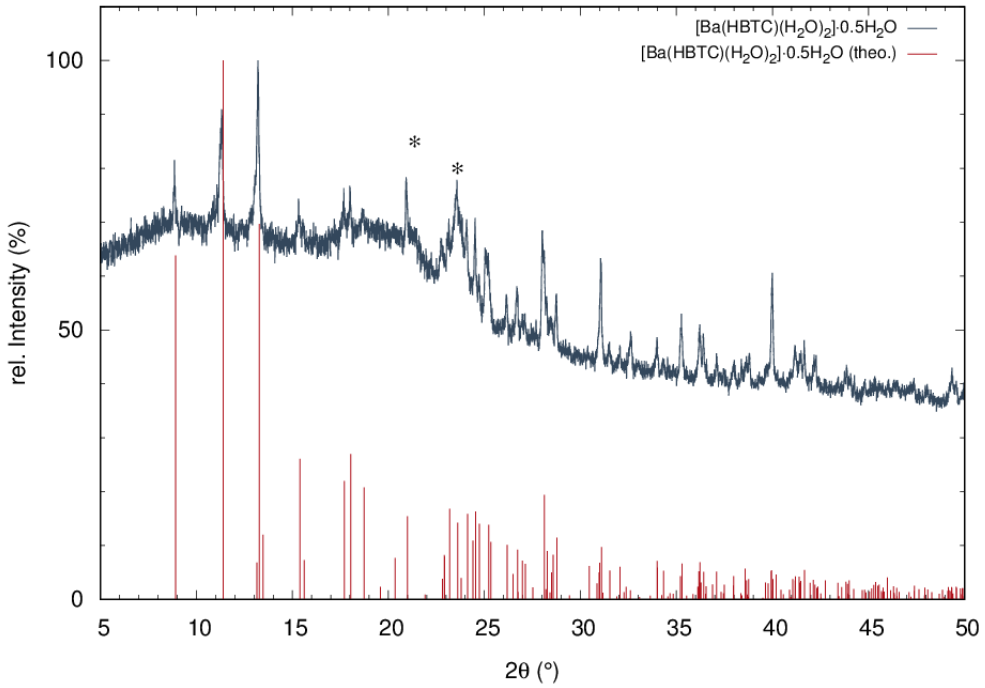

Figure S11. XRPD pattern of $^{3}_{\infty}$[Ba(HBTC)$(H_2O)_2$]·½ H_2O (**3**) (blue curve; Huber G670, Cu-$K_{\alpha 1}$ radiation). For comparison the theoretical pattern calculated from single crystal data is shown (red line diagram). Reflections of the sample holder are marked with a "*".

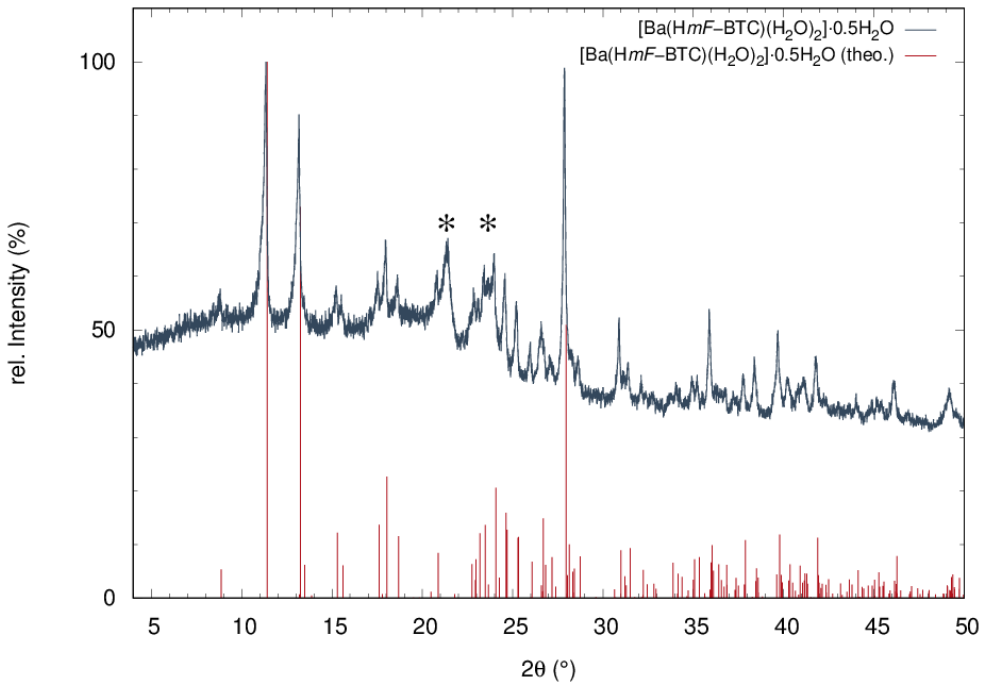

Figure S12. XRPD pattern of $^{3}_{\infty}$[Ba(H*mF*-BTC)$(H_2O)_2$]·½ H_2O (**4**) (blue curve; Huber G670, Cu-$K_{\alpha 1}$ radiation). For comparison the theoretical pattern calculated from single crystal data is shown (red line diagram). Reflections of the sample holder are marked with a "*".

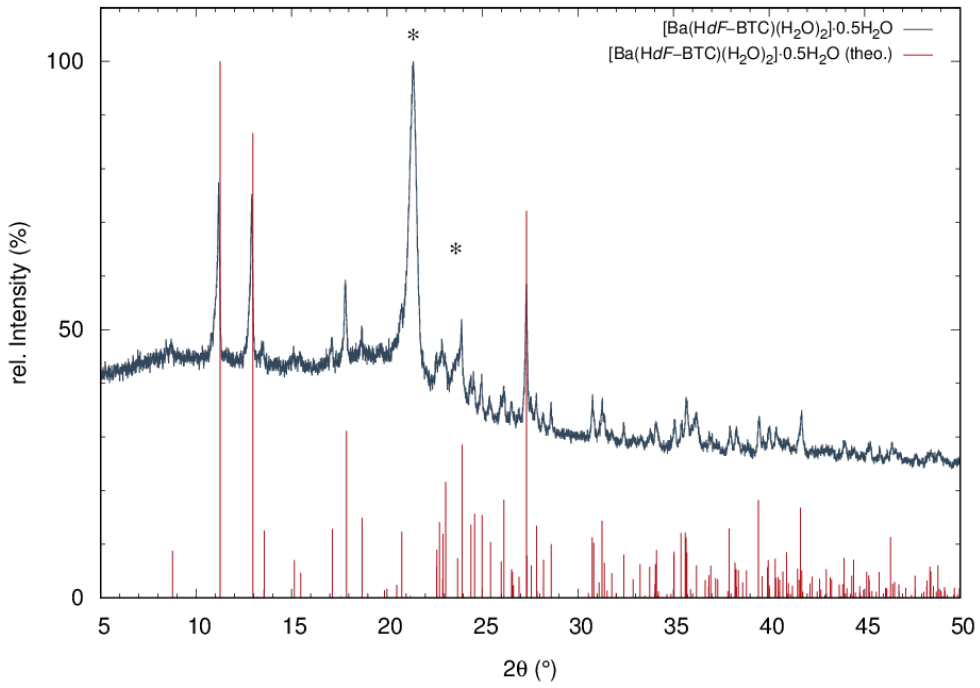

Figure S13. XRPD pattern of $^{3}_{\infty}$[Ba(H*dF*-BTC)(H_2O)$_2$]·½ H_2O (**5**) (blue curve; Huber G670, Cu-$K_{\alpha 1}$ radiation). For comparison the theoretical pattern calculated from single crystal data is shown (red line diagram). Reflections of the sample holder are marked with a "*".

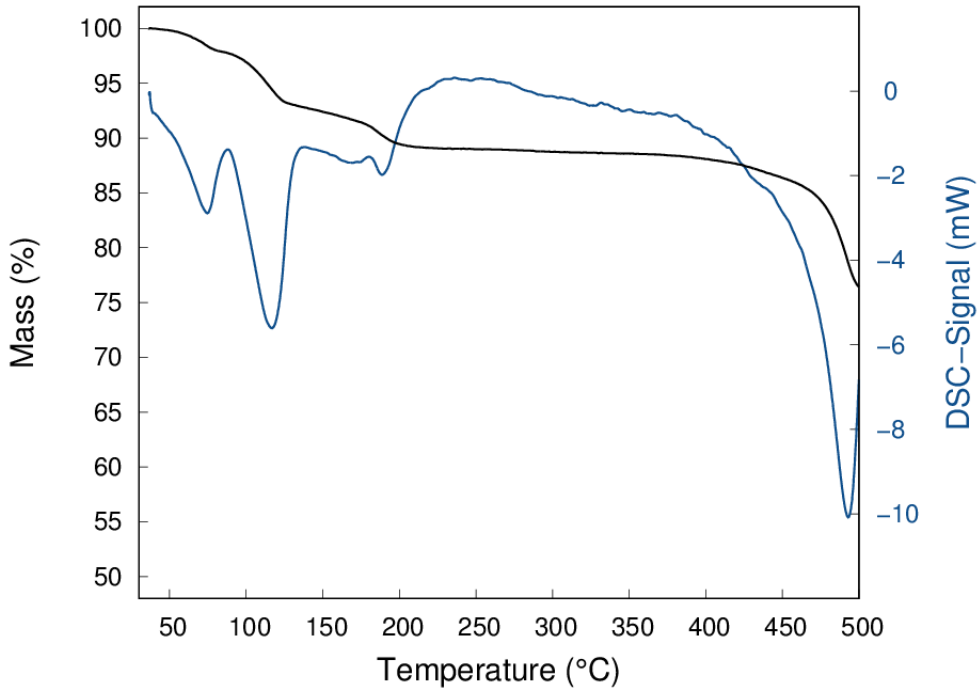

Figure S14. DSC (blue) and TG (black) curves of $^{3}_{\infty}$[Ba(HBTC)(H_2O)$_2$]·½ H_2O (**3**).

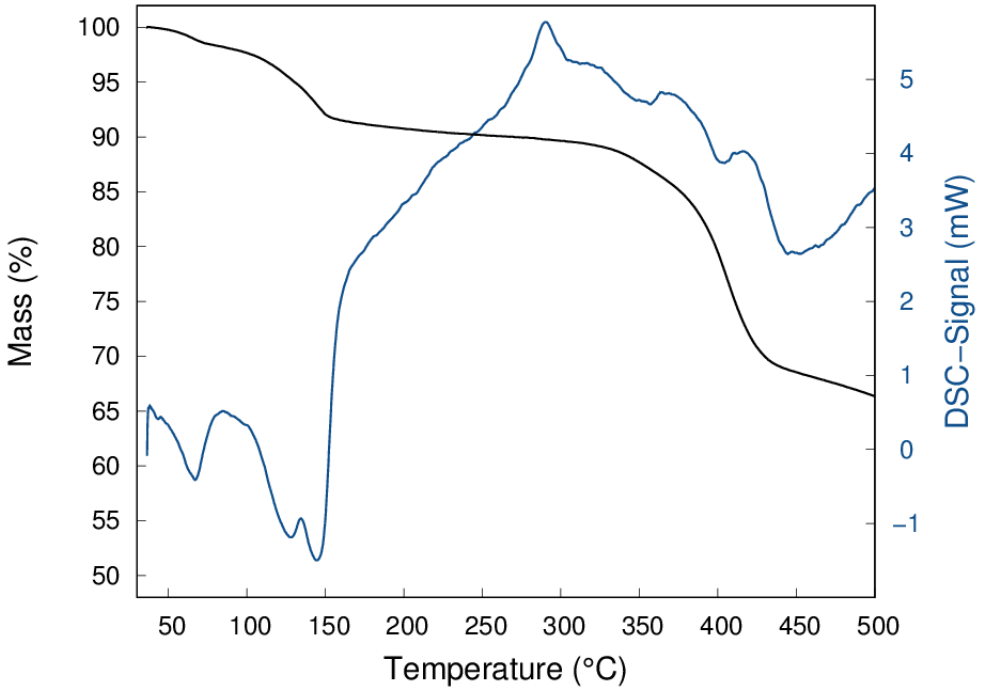

Figure S15. DSC (blue) and TG (black) curves of $^{3}_{\infty}$[Ba(H*mF*-BTC)$(H_2O)_2$]·½ H_2O (**4**).

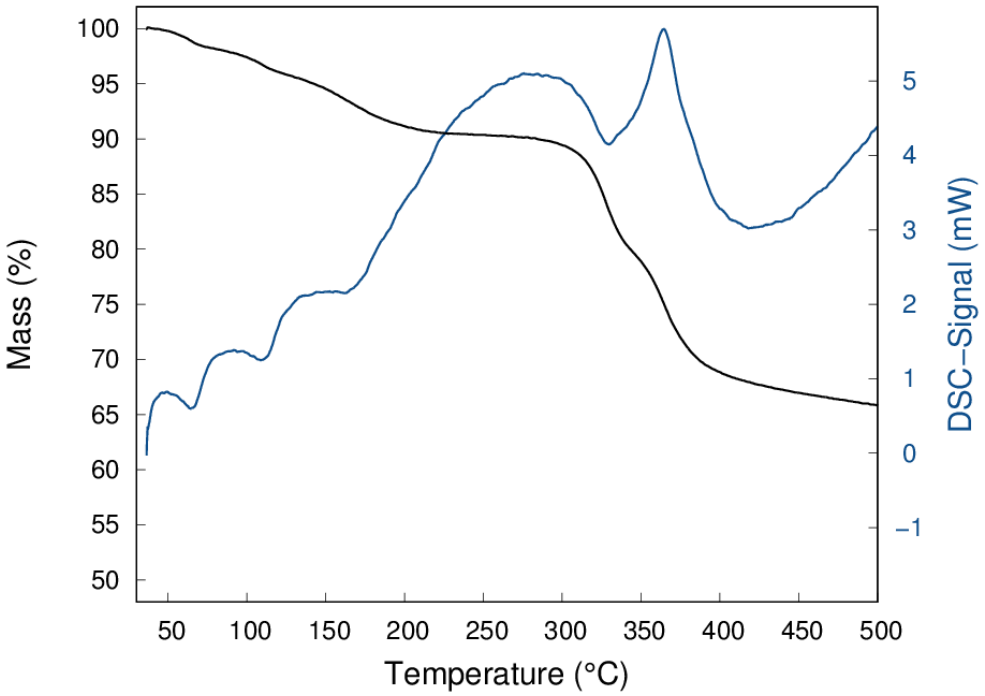

Figure S16. DSC (blue) and TG (black) curves of $^{3}_{\infty}$[Ba(H*dF*-BTC)$(H_2O)_2$]·½ H_2O (**5**).

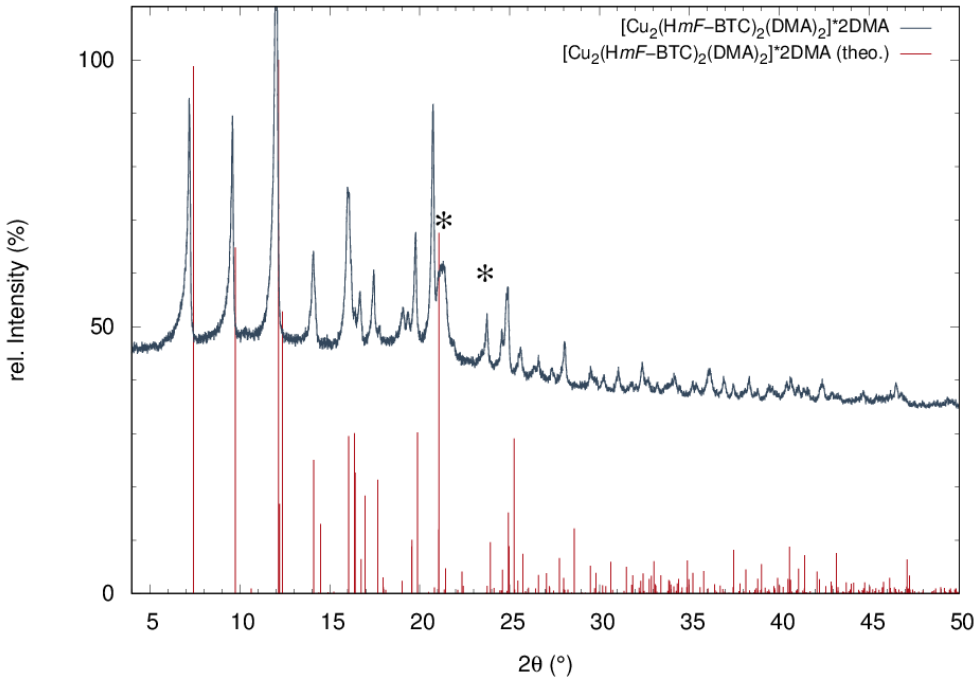

Figure S17. XRPD pattern of UHM-33 ($^{2}_{\infty}$[Cu_2(H*mF*-BTC)$_2$(DMA)$_2$]·2 DMA, **6**) (blue curve; Huber G670, Cu-$K_{\alpha1}$ radiation). For comparison the theoretical pattern calculated from single crystal data is shown (red line diagram). Reflections of the sample holder are marked with a "*".

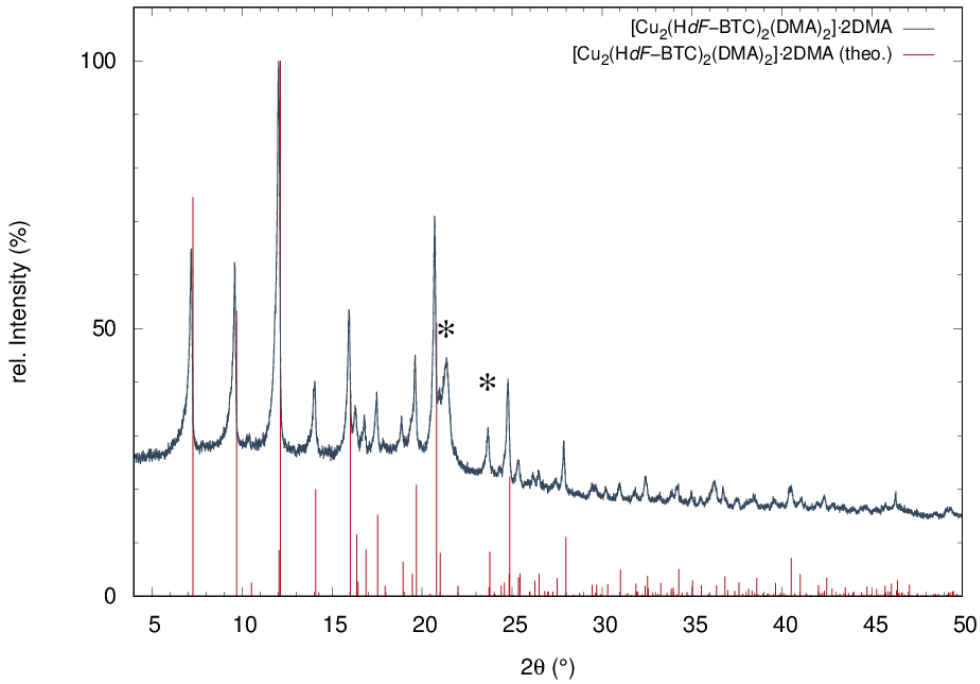

Figure S18. XRPD pattern of *dF*-UHM-33 ($^{2}_{\infty}$[Cu_2(H*dF*-BTC)$_2$(DMA)$_2$]·2 DMA, **7**) (blue curve; Huber G670, Cu-$K_{\alpha1}$ radiation). For comparison the theoretical pattern calculated from single crystal data is shown (red line diagram). Reflections of the sample holder are marked with a "*".

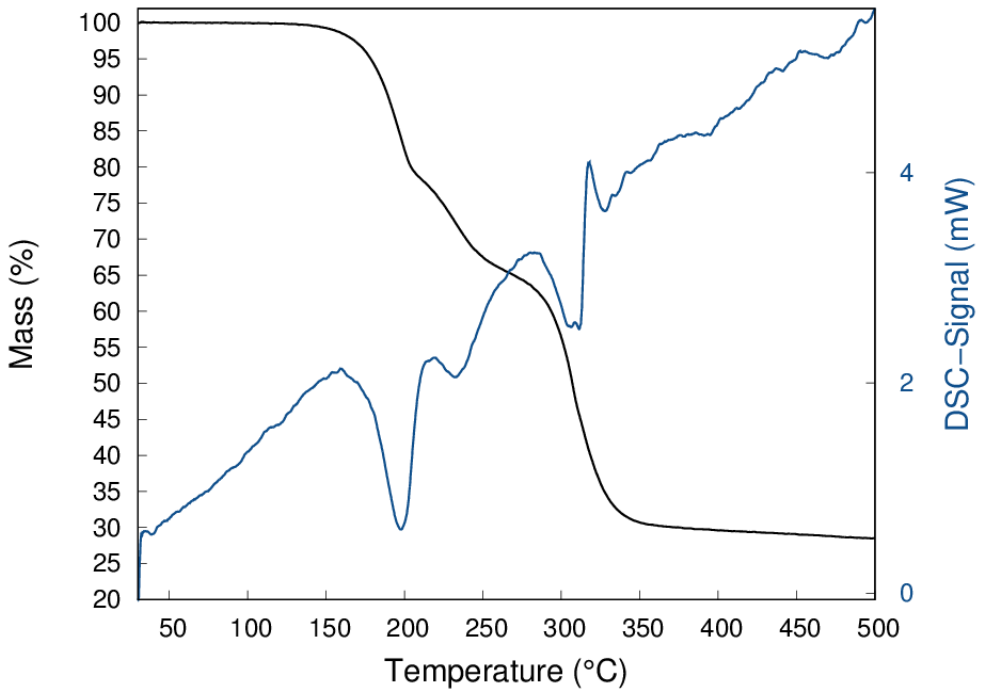

Figure S19. DSC (blue) and TG (black) curves of UHM-33 ($^{2}_{\infty}$[Cu_2(H*mF*-BTC)$_2$(DMA)$_2$]·2 DMA, **6**).

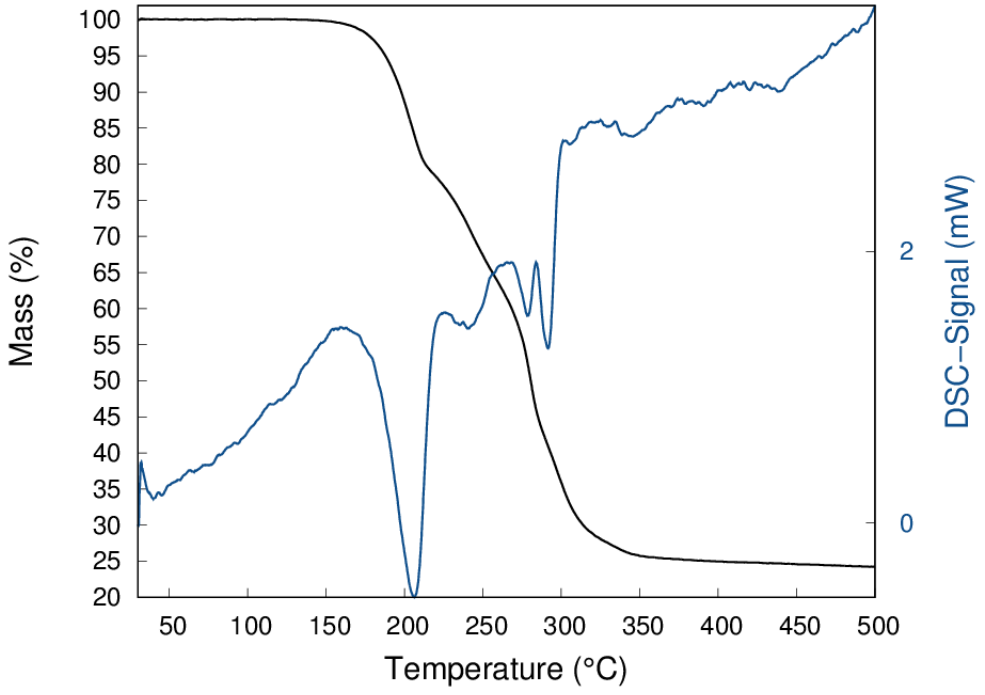

Figure S20. DSC (blue) and TG (black) curves of *dF*-UHM-33 ($^{2}_{\infty}$[Cu_2(H*dF*-BTC)$_2$(DMA)$_2$]·2 DMA, **7**).